JOURNAL OF GEOPHYSICAL RESEARCH, VOL. 98, NO. C12, PAGES 22,629–22,644, DECEMBER 15, 1993

Estimating Global Air-Sea Fluxes From Surface Properties And From Climatological Flux Data Using an Oceanic General Circulation Model

ELI TZIPERMAN

Environmental Sciences and Energy Research, Weizmann Institute of Science, Rehovot, Israel

KIRK BRYAN

Geophysical Fluid Dynamics Laboratory, Princeton University, Princeton, New Jersey

A simple method is presented and demonstrated for estimating air-sea fluxes of heat and fresh water with the aid of a general circulation model (GCM), using both sea surface temperature and salinity data and climatological air-sea flux data. The approach is motivated by a least squares optimization problem in which the various data sets are combined to form an optimal solution for the air-sea fluxes. The method provides estimates of the surface properties and air-sea flux data that are as consistent as possible with the original data sets and with the model physics. The calculation of these estimates involves adding a simple equation for calculating the air-sea fluxes during the model run and then running the model to a steady state. The proposed method was applied to a coarse resolution global primitive equation model and annually averaged data sets. Both the spatial distribution of the global air-sea fluxes and the meridional fluxes carried by the ocean were estimated. The resulting air-sea fluxes seem smoother and significantly closer to the climatological flux estimates than do the air-sea fluxes obtained from the GCM by simply specifying the surface temperature and salinity. The better fit to the climatological fluxes was balanced by a larger deviation from the surface temperature and salinity. These surface fields were still close to the observations within the measurement error in most regions, except western boundary areas. The inconsistency of the model and data in western boundary areas is probably related to the inability of the coarse resolution GCM to appropriately simulate the large transports there. The meridional fluxes calculated by the proposed method differ very little from those obtained by simply specifying the surface temperature and salinity. We suggest therefore that these meridional fluxes are strongly influenced by the interior model dynamics; in particular, the too-weak model meridional circulation cell seems to be the reason for differences between the meridional transports in the model and those estimated from other sources. We discuss the implications for the calculation of air-sea fluxes by inverse models.

1. INTRODUCTION

The recent interest in climate and, in particular, in the ocean's role in the climate system has increased the need to obtain accurate estimates of air-sea fluxes of heat and fresh water. Such estimates are needed both for driving ocean models and for monitoring the changes in the air-sea fluxes due to a possible climate change. The available estimates of these fluxes are obtained from various sources, all of which have well-known limitations. In particular, climatological flux estimates obtained from meteorological ship data with the aid of empirical bulk formulas [*Esbensen and Kushnir*, 1981; *Baumgartner and Reichel*, 1975] are known to contain large uncertainties.

Ocean models and oceanographic data are commonly believed to be among the more reliable sources for estimates of air-sea fluxes of heat and fresh water and of the related meridional fluxes carried by the oceans. The "direct method" [e.g., *Bryan*, 1962; *Hall and Bryden*, 1982] uses hydrographic data and dynamic calculations, possibly with the addition of current meter measurements in western boundary currents, to calculate the fluxes of heat and salt carried by the ocean and the air-sea fluxes. However, flux estimates obtained by the direct method contain uncertainties due to improper temporal and spatial resolution of the data, particularly in western boundary regions, and to the level of no motion assumption. Inverse methods may be used to avoid the level of no motion assumption [*Wunsch*, 1984]. However, the dynamics often used in inverse models, geostrophy and box conservation of mass heat and salt, is very simplified. It is clearly desirable to use more complex (and hopefully more accurate) dynamics for estimating the surface fluxes. It is also necessary to use methods of analysis that can compensate for data errors due to incomplete sampling. However, newly introduced inverse methods which allow the use of fully complex general circulation models (GCMs) are still being developed [*Tziperman et al.*, 1992] and are quite difficult to implement and use.

Ocean general circulation models can produce estimates of air-sea fluxes if given the surface distributions of temperature and salinity, although there are several difficulties with this approach as well. First, the resulting fluxes tend to have spatial distributions that are too noisy. In addition, the resulting air-sea fluxes and related meridional fluxes carried by the ocean are often inconsistent with other flux estimates, such as climatological fluxes obtained from meteorological ship data. An important yet unanswered question is whether the fluxes calculated by oceanic GCMs can be made consistent with the other flux estimates by changing the specified surface temperature and salinity within the error estimates for the surface property data. Finally, in specifying surface

Paper number 93JC01139.
0148-0227/93/93JC-01139$05.00

properties in a GCM simulation in order to calculate the air-sea fluxes, the existing air-sea flux estimates from atmospheric models or climatological ship data are normally not used, so that the resulting air-sea flux estimate is not optimal because not all of the available information was used to obtain it.

This work has two main objectives. The first is to propose a simple method for calculating air-sea fluxes by combining data of the sea surface temperature (SST) and sea surface salinity (SSS) with climatological estimates of the air-sea fluxes, using an oceanic general circulation model. The method is demonstrated using a realistic complex general circulation model of the global ocean, by producing global estimates of the air-sea fluxes. Our second objective is to examine the consistency of the model and various data sets (surface temperature and salinity and climatological flux data). More specifically, we wish to determine whether these various data sets are consistent with each other and with the model dynamics and to locate the sources of possible inconsistencies. We shall demonstrate that by allowing the model to deviate from the data for the surface temperature and salinity within the assumed observational errors, it is possible to make the air-sea fluxes calculated by the model more consistent with the climatological flux data. Yet the model meridional fluxes carried by the ocean will be shown to be less sensitive to the details of the surface temperature and salinity than the climatological fluxes. In fact, the model meridional transports are significantly different from those derived from the climatological flux data, even when we allow the model to deviate from the surface temperature and salinity data. In this context, we are particularly interested in locating specific model limitations that cause the inconsistencies between the model and the various data sets. Thus the present approach is used for validating the model as well as for obtaining the flux estimates. (The model validation is done simultaneously with the flux estimation by simply examining the residual fields when calculating the optimal fluxes.)

The method proposed here offers several advantages over those mentioned above. First, both sea surface property data and existing flux estimates are used to obtain the desired estimate of the air-sea fluxes. Each data type is weighted by its error level, so that the more accurate data are given larger weight. Another advantage is that the model equations used to estimate the air-sea fluxes may be as complex as desired, and we demonstrate the method using a global primitive equation model. In addition, the method allows the model to deviate from the specified surface temperature and salinity in order to better fit the existing flux estimates. Finally, the estimated fluxes are consistent with the steady state model dynamics. In particular, for the global model used in this study, the total integrated air-sea fluxes of heat and fresh water vanish, as no net gain by the ocean of heat and fresh water is allowed at steady state. Important information is provided by the residual fields, i.e., the difference between the calculated surface properties and the corresponding data and the difference between the calculated air-sea fluxes and the corresponding data. By examining these residual fields, it is possible to determine in what regions the surface property and climatological flux estimates are consistent with each other and with the model dynamics within the a priori error bars.

The procedure used here is motivated by an optimization (inverse) approach, yet it is far simpler to implement than nonlinear inverse methods that can, in principle, be used for this purpose. The very simple equations used in the GCM to calculate the air-sea fluxes are similar to the one-way feedback used in ocean models as upper boundary conditions [*Oberhuber*, 1988; *Ezer and Mellor*, 1991].

The following sections describe the methodology, model, and data (section 2) and the results of a calculation of the heat and freshwater fluxes using a global primitive equation model and global data sets (section 3). Conclusions are presented in section 4.

2. METHODOLOGY, MODEL, AND DATA

2.1. *Methodology*

Oceanographic general circulation models use one of two alternative formulations of the upper boundary condition for temperature and salinity. In one formulation, climatological heat flux data H^d and evaporation minus precipitation data $(E - P)^d$ are used to drive the model, while in the other, sea surface temperature SST and sea surface salinity SSS are specified through a Rayleigh type condition.

The surface temperature is specified in an oceanic GCM by driving the model with an implied air-sea heat flux H^{SST} that is calculated from the model upper level temperature $T_{i,j,k=1}$ and the temperature data at this depth, $T^d_{i,j,k=1}$ (where the indices i and j denote horizontal grid point location, and k denotes vertical level), as follows:

$$H^{\mathrm{SST}}_{ij} = \rho_0 C_p \gamma^T \Delta z_1 (T^d_{i,j,k=1} - T_{i,j,k=1}). \qquad (1)$$

The restoring coefficient γ^T has units of 1 over time, C_p is the heat capacity of seawater, ρ_0 is a constant reference density, and Δz_1 denotes the thickness of the upper model level. Similarly, an implied freshwater flux is calculated from the difference of the model surface salinity and the surface salinity data,

$$(E - P)^{\mathrm{SSS}}_{ij} = \gamma^S \Delta z_1 (S^d_{i,j,k=1} - S_{i,j,k=1})/S_0, \qquad (2)$$

where S_0 is a constant reference salinity used to convert the virtual salt flux to an implied freshwater flux.

Both the climatological flux data and the implied fluxes derived from a GCM clearly cannot be considered optimal, as each of them ignores some of the available information (SST or H^d) that can be used to calculate the air-sea fluxes. Given data of both the sea surface properties (SST^d and SSS^d) and the air-sea fluxes (H^d and $(E - P)^d$), it is desirable to use them together in order to calculate an optimal estimate for the poorly known air-sea fluxes. The two types of data must be combined through a model to form optimal air-sea flux estimates. The optimal estimates of the air-sea fluxes of heat H and fresh water $(E - P)$ can be solved for by formulating an appropriate optimization problem. The optimal estimates must be as consistent as possible with both the flux data and the implied fluxes calculated by a GCM from the surface temperature and salinity data. The model equations are used as constraints, such that the model is driven by the fluxes H and $(E - P)$, and the resulting model solutions for the sea surface temperature and salinity are used (through (1) and (2)) to calculate the implied fluxes H^{SST} and $(E - P)^{\mathrm{SSS}}$. The solution to this optimization problem minimizes a cost function of the form

$$\mathbf{J}[\mathrm{SST}, H, \mathrm{SSS}, (E-P)] = \sum_{ij} \{W^{\mathrm{SST}}(H_{ij}^{\mathrm{SST}} - H_{i,j})^2 + W^H(H_{i,j}^d - H_{i,j})^2 + W^{\mathrm{SSS}}[(E-P)_{ij}^{\mathrm{SSS}} - (E-P)_{i,j}]^2 + W^{[E-P]}[(E-P)_{i,j}^d - (E-P)_{i,j}]^2\}. \quad (3)$$

Note that the terms involving H^{SST} and $(E-P)^{\mathrm{SSS}}$ serve simply to constrain the model surface temperature and salinity to be close to the observed SST^d and SSS^d. The rationale for this form of the cost function is discussed further, following (11). The weights (W^{SST}, etc.) in the cost function are chosen to be proportional to the squared inverse error for each of the data fields. The weights could, in general, be functions of location if information on the spatial structure of the errors is available, or they could even be represented by nondiagonal matrices in order to represent information of the spatial error covariance. The minimization problem posed by (3) could, in principle, be solved using various nonlinear inverse methods (linear methods cannot be used because the model equations used as constraints are nonlinear), such as the adjoint method [*Tziperman et al.*, 1992] or others [*Mercier*, 1989]. We wish, however, to present here a simpler alternative for combining surface property and air-sea flux data using an oceanic GCM. After presenting this simpler methodology, we shall discuss its relation to the optimization problem (3).

Because we want to obtain a heat flux estimate that is as close as possible to both the flux calculated by specifying surface properties (H^{SST}) and the available climatological heat flux data H^d, we simply write the optimal flux as a weighted average of the two:

$$H = \alpha^T H^d + (1-\alpha^T)H^{\mathrm{SST}}, \quad (4)$$

$$(E-P) = \alpha^S(E-P)^d + (1-\alpha^S)(E-P)^{\mathrm{SST}}. \quad (5)$$

As we wish to weight the two terms in the weighted average expression for the heat flux by their corresponding errors, $\varepsilon(H^d)$ and $\varepsilon(H^{\mathrm{SST}})$, we choose

$$\alpha^T/(1-\alpha^T) = \varepsilon(H^{\mathrm{SST}})/\varepsilon(H^d), \quad (6)$$

$$\alpha^S/(1-\alpha^S) = \varepsilon[(E-P)^{\mathrm{SSS}}]/\varepsilon[(E-P)^d]. \quad (7)$$

Note that if H^{SST} and H^d were independent, the least squares optimal estimate would require that the weight ratio $\alpha^T/(1-\alpha^T)$ be proportional to the square ratio of the corresponding errors [e.g., *Ghil and Malanotte-Rizzoli*, 1991]. These fluxes are not independent, however, so the simple least squares optimal estimate cannot be used. The dependence of the fluxes is an important issue: H^{SST} is calculated every time step during the model run, based on the model SST that is in turn affected by the value of H which is calculated from H^{SST} by (4). The dependence of H^{SST} and H implies that one cannot simply run the model under restoring conditions, find H^{SST}, and then use (4) to calculate the optimal H. As a result, if $\alpha^T = 0.9$, for example, we do not expect the optimal flux to necessarily be much closer to H^{SST} than to H^d. All that can be expected is that the rms deviation between the optimal flux and the flux data, and the rms deviation between the model SST and the SST data, will be within the error estimate used to calculate α^T. Note that if $\alpha^T = \alpha^S = 0$, as is the case in some of the runs presented below, (4)–(7) simply reduce to using the usual restoring conditions. Equations (6) and (7) are further justified below by examining their relation to the cost function (3).

The error estimate for the surface temperature data is $\varepsilon(T) = 1°$, and the corresponding surface salinity error is $\varepsilon(S) = 0.25$ parts per thousand (ppt). These errors represent measurement and sampling errors, as well as errors due to the unresolved seasonal signal. While precise estimates for these errors cannot be given, we consider the values given above to be reasonable order of magnitude estimates. Using (1) and (2) to translate SST and SSS errors into an error estimate for the implied heat fluxes, we have

$$\varepsilon(H^{\mathrm{SST}}) = \rho_0 C_p \gamma^T \Delta z_1 \varepsilon(T) = 81 \text{ W m}^{-2}, \quad (8)$$

$$\varepsilon[(E-P)^{\mathrm{SSS}}] = \gamma^S \Delta z_1 \varepsilon(S)/S_0 = 434 \text{ cm yr}^{-1}, \quad (9)$$

where we have used $\gamma^{T,S} = 1/30 \text{ days}^{-1}$, $C_p = 4185 \text{ J kg}^{-1}$ $°\text{C}^{-1}$, $S_0 = 35$ ppt, and $\Delta z_1 = 50$ m. The high value for the error in the implied salt flux indicates that γ^S should probably be chosen smaller than $1/30 \text{ days}^{-1}$ when driving an oceanic GCM by specifying the surface salinity, which is further discussed below (see (15)). Note that the error in H^{SST} and $[E-P]^{\mathrm{SSS}}$ is in large part due to model errors, not only errors in the SST and SSS data. Model errors are, of course, even more difficult to quantify than data errors, but if given any information on these errors, they could be included in $\varepsilon(H^{\mathrm{SST}})$.

Error estimates for climatological air-sea fluxes vary significantly among different sources. As a reasonable estimate for the error in the heat flux data, one can choose 50 W m^{-2} [e.g., *Tally*, 1984]. Errors for the evaporation are of the order of 25%, while the errors for the precipitation may be much larger [*Wijffels et al.*, 1992]. We therefore choose the following rough order of magnitude error estimates:

$$\varepsilon(H^d) = 50 \text{ W m}^{-2},$$

$$\varepsilon[(E-P)^d] = 50 \text{ cm yr}^{-1}. \quad (10)$$

These error estimates are clearly somewhat uncertain, but note that only the ratios of the error estimates for the surface temperature (salinity) and for the climatological heat (freshwater) fluxes enter the calculations α^T and α^S.

With these error estimates we obtain the value of the coefficients in the expressions (4) and (5) for the fluxes:

$$\alpha^T = 0.6; \qquad \alpha^S = 0.9. \quad (11)$$

The larger value found for α^S indicates that because γ^S was chosen to be relatively large, less weight is given to the implied flux calculated from the surface salinity distribution when combining the implied and climatological fluxes into a single estimate. In general, the error estimates in (8) and (9) are clearly strongly dependent on the choice of the restoring coefficient γ, reflecting the arbitrariness of these coefficients in calculations of air-sea fluxes from surface properties using ocean GCMs. Note, however, that this arbitrariness is at least partially removed in the present approach; a too-large restoring coefficient is automatically compensated by an appropriate value of α^T or α^S.

In order to better understand the formulation in (4) and (5) (or (3)) for estimating the air-sea fluxes by combining SST and climatological flux data sets, let us first examine the case

where the errors in the SST data are vanishingly small (or equivalently, where those in the climatological flux data are very large). In this case, we find from (6) that $\alpha^T = 0$, and our formulation (4) reduces to using the standard restoring boundary conditions, $H = H^{SST}$. The restoring boundary conditions tend to make the model SST close to the SST data. However, it is important to understand that although we assume perfect SST data in this case, the model SST will not be equal to the data for the SST. The two will still be different, and the resulting air-sea heat flux (equation (1)) that is proportional to the difference between them will not vanish. The distance between the model SST and the SST data is determined by the restoring coefficient γ^T. The better model we use, and the higher its resolution, the larger we can choose γ^T, and the closer the model SST will be to the corresponding SST data. The difference between the model SST and the corresponding data may be viewed as a result of model errors that do not enable the model to fit perfectly the observed SST. It is therefore unwise to choose γ^T or γ^S to be too large for a coarse model, as this results in very noisy and unreasonable values for the implied fluxes, as will be seen below for the implied freshwater fluxes. While γ^T increases and the difference $SST^d - SST$ decreases, their product remains finite and provides the desired air-sea flux estimate. With a perfect model and noise-free SST and air-sea flux data, the implied fluxes should be perfectly consistent with the climatological flux estimates. In a more realistic situation, when the model and the various data sets are not completely consistent, the term $(H_{ij}^{SST} - H_{i,j})^2$ in the cost function (3) simply serves to enforce the model surface temperature to be close to the SST data. When the errors in the SST data are not negligible, α^T does not vanish, and both SST^d and H^d are utilized by our approach. The model is then allowed to deviate further from the SST data in order to better fit the climatological flux data H^d. Clearly, in this case, too, the SST data and the model SST will never be equal but will get only as close as is allowed by the specified SST errors and the restoring coefficient γ^T.

The derivation of the equations for the air-sea fluxes based on both the sea surface property data and the climatological flux data is now completed. We now wish to further justify our approach in (4) and (5) by briefly discussing its relation to the optimization problem stated in (3). (The reader interested mostly in the results can now skip to section 3.) *Tziperman et al.* [1992] have shown that the robust diagnostic method of *Sarmiento and Bryan* [1982] may be seen as a special limit of an optimization approach that seeks to combine model dynamics and hydrographic data by minimizing an appropriate cost function. Similarly, we would like to suggest that the solution to the air-sea fluxes obtained from our equations (4) and (5) is closely related to the minimum solution of the cost function (3).

To see the relation between the optimization problem and the equations we derived, consider again the cost function (3). The weights in front of each of the terms in the cost function represent the inverse squared error for each term. At the minimum of the cost function the temperature field, for example, is expected to deviate from the data value by about the error estimate. As a result, the value of $(T - T^d)^2$ is roughly the value of the error squared, so that when normalized by the number of data points, the term $\sum W^T (T - T^d)^2$ is expected to be of order 1. Similarly, at the minimum of the cost function each of the terms in the cost function is of order 1 after normalizing by the number of data points, so that we expect the different terms of the cost function to have roughly the same magnitudes (see *Tziperman et al.* [1992] for additional details). The temperature terms, for example, should therefore satisfy

$$\sum_{ij} [W^{SST}(H_{ij}^{SST} - H_{i,j})^2] \approx \sum_{ij} [W^H(H_{i,j}^d - H_{i,j})^2]. \quad (12)$$

Next, without rigorous justification, but based on the experience of *Tziperman et al.* [1992] with a similar problem, we translate this condition into a local balance:

$$W_{ij}^{SST}(H_{ij}^{SST} - H_{i,j})^2 \approx W_{ij}^H(H_{i,j}^d - H_{i,j})^2. \quad (13)$$

This local balance is clearly not expected to hold exactly in a least squares problem based on the cost function (3), but it is used here merely to justify (4) and (5). Taking the square root of the last equation and assuming that the numerical value of the optimal heat flux H is between those of the implied flux H^{SST} and the climatological data H^d, we have

$$[W^{SST}/W^H]^{1/2}(H_{ij}^{SST} - H_{i,j}) \approx (H_{i,j} - H_{i,j}^d). \quad (14)$$

A final manipulation of (14) brings us to the form postulated before in (4), and the relation between the weights in the cost function (3) and the coefficient α^T can be easily shown to be

$$\alpha^T = [1 + (W^H/W^{SST})^{1/2}]^{-1}. \quad (15)$$

With $W^H = 1/\varepsilon(H^d)^2$ and $W^{SST} = 1/\varepsilon(H^{SST})^2$, (15) is consistent with our recipe (equation (6)) for choosing α^T. Both the form of (14) and the value of the weight α^T therefore demonstrate the link between the optimization problem of (3) and the one solved by our approach in (4) and (5). Although the results of the two methodologies cannot be expected to be equal, they may be expected to be fairly close. The simple approach used here can be used to initialize a least squares optimization based on a more rigorous nonlinear inverse method such as the adjoint method. Such an initialization is important because the gradient-based optimization methods may fail if they are started too far from the optimal solution because of the possible existence of multiple local minima of the cost function [*Tziperman et al.*, 1992].

It is interesting to note that the equations used in the GCM to calculate the air-sea fluxes are similar to the one-way feedback used in ocean models as upper boundary conditions [*Oberhuber*, 1988; *Ezer and Mellor*, 1991]. The major difference is that there the choice of coefficients is not based on the error estimates of the surface properties and flux data but on quite different considerations.

The proposed methodology was implemented in the general circulation model, which was run to a steady state (typically integrating for 1500 years, using different time steps for the tracer and momentum equations, as well as for the deep and upper ocean in order to accelerate the convergence to steady state [*Bryan*, 1984]). The globally integrated fluxes of heat and fresh water were examined to make sure that the average net input of heat and fresh water into the ocean at steady state is sufficiently small (typically less than 0.1 W m^{-2} and 0.1 cm yr^{-1}). The zero net air-sea flux is easily obtained here, but it may require an explicit additional constraint in an inverse calculation based on the cost function (3).

2.2. *Data*

In order to demonstrate the methodology discussed above, we have chosen to use a coarse resolution global

primitive equations model, together with annually averaged climatological data. The *Levitus* [1982] data are used for the temperature and salinity at the depth of the first model level (Figures 1*a* and 1*b*); the heat flux data used here are those of *Esbensen and Kushnir* [1981] and are shown in Figure 1*c*; evaporation minus precipitation minus runoff data are taken from *Baumgartner and Reichel* [1975] (Figure 1*d*). Finally, Figure 1*e* shows the meridional heat and freshwater fluxes derived from the climatological flux data, using the expression given on the right-hand side of (17). Both the spatial distribution of the air-sea fluxes and the derived meridional fluxes will be later compared with the results of our calculation. Error estimates for climatological air-sea fluxes of heat and fresh water were discussed, for example, by *Tally* [1984] and *Wijffels et al.* [1992]. The error information needed in the calculation presented below has been specified as discussed in the section 2.1. Finally, the wind stress used here is the annually averaged *Hellerman and Rosenstein* [1983] data.

2.3. *Model*

The general circulation model used in this study has been used in several previous studies, in which it was coupled with an atmospheric model [*Stouffer et al.*, 1989; *Manabe et al.*, 1991]. A model of higher horizontal and vertical resolution would have been preferred, but that would have made an exploration of parameters more difficult. The model is of the annually averaged ocean circulation and does not resolve the seasonal cycle. There are two main justifications for using a steady model here. First, we find below that the results from this model are not very different from the annually averaged results of previous similar seasonal models. In addition, we prefer to test the suggested methodology on a simpler steady model before proceeding to the more complex seasonal case. The basic model is similar to that of *Bryan* [1969] with later modifications by *Semtner* [1974] and *Cox* [1984]. The parameters and vertical structure are similar to those used by *Bryan and Lewis* [1979] in an early study of the world ocean. A special feature of the present model is the inclusion of a mixing tensor, which allows lateral mixing of heat and salt to be tilted so that it is aligned at some angle between the horizontal and a plane parallel to surfaces of constant density. Since the tensor diffusivity formulation of this model has not been documented elsewhere, we provide its description in the appendix with the important parameters of the model.

For this study we have allowed for an exchange of water between the Atlantic and Pacific oceans, by specifying a flow of 0.75 Sv (1 Sv = 10^6 m^3 s^{-1}) through the Bering Strait, following the recent measurements by *Coachman and Aagaard* [1988]. In addition, the exchange between the Pacific and Indian oceans through the Indonesian straits, for which estimates vary between 1–2 Sv and 20 Sv, was specified here to be 4 Sv. In both cases, the specification involves setting the barotropic stream function to a fixed value, while allowing the model to adjust the baroclinic component of the flow. The consequences of allowing for these interocean exchanges, particularly between the Atlantic and Pacific oceans, have been examined in detail by *Wijffels et al.* [1992] and are discussed further below.

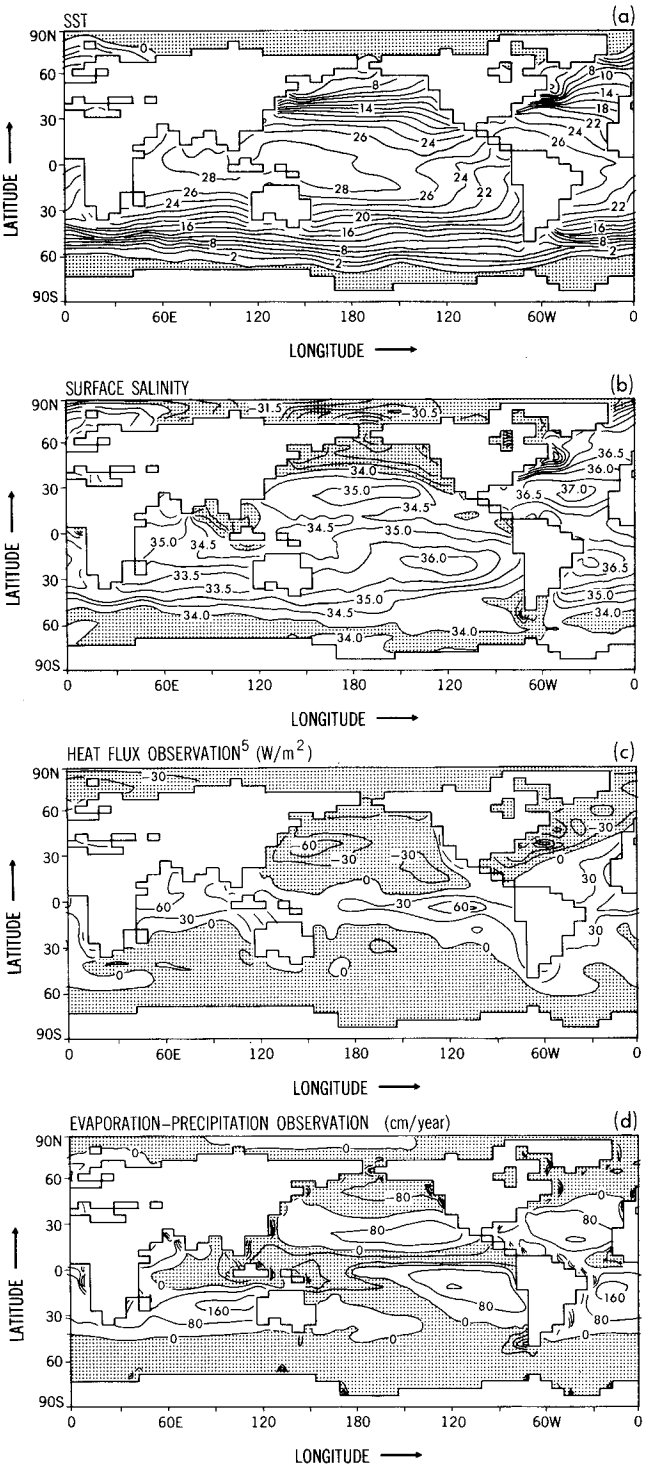

Fig. 1. (*a*) The *Levitus* [1982] temperature at the depth of the upper tracer grid point in the model (25 m). (*b*) Levitus salinity at 25 m. (*c*) Annually averaged *Esbensen and Kushnir* [1981] heat flux. (*d*) *Baumgartner and Reichel* [1975] annually averaged ($E - P$ runoff). (*e*) Global meridional heat and freshwater fluxes calculated from the Baumgartner and Reichel and Esbensen and Kushnir data sets. The labels on the curves indicate transports in the Atlantic Ocean (dotted lines marked A) and in the Pacific and Indian oceans combined (dashed lines marked P & I), and the total global ocean meridional transports (solid lines marked T).

2.4. *Meridional Fluxes of Heat and Fresh Water*

Among the useful diagnostic tools used to discuss the results of the calculation of the air-sea fluxes are the meridional fluxes of heat and fresh water carried by the ocean. Let x, y, and z and u, v, and w be the eastward, northward, and vertical coordinates and velocities, respectively; let k_v and k_h be the vertical and horizontal diffusivities of heat, respec-

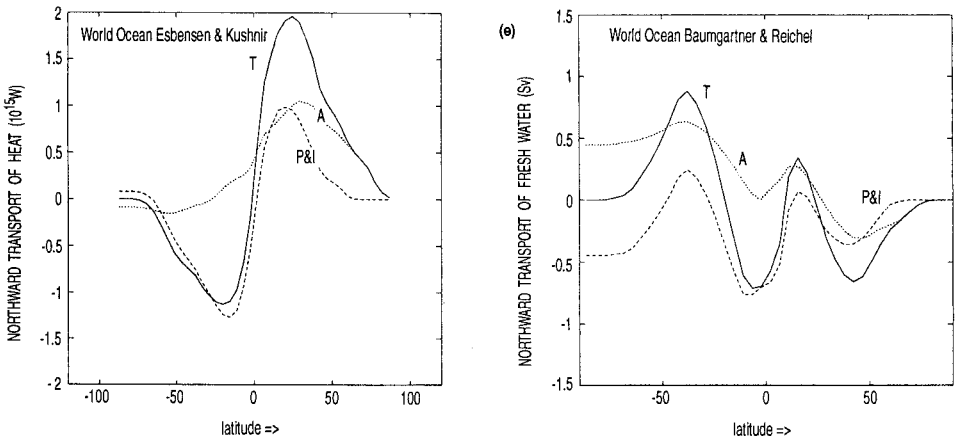

Fig. 1. (continued)

tively; and consider the advection-diffusion equation for the temperature:

$$(uT)_x + (vT)_y + (wT)_z - (k_v T_z)_z - [(k_h T_x)_x + (k_h T_y)_y] = 0. \quad (16)$$

Integrating this equation over a longitudinal section of a closed basin (i.e., over x and z) and from some latitude y_0 to latitude y, using integration by parts, the surface boundary condition $\rho_0 C_p k_v T_z = H$, and the no-flux and no-flow conditions on the bottom, east, and west boundaries, we find

$$\left[\int\int dx\, dz \rho_0 C_p (vT - k_h T_y)\right]\Bigg|_{y_0}^{y} = \int\int_{y_0}^{y} dx\, dy' H. \quad (17)$$

The left-hand side represents the difference in the total meridional heat flux (advective and diffusive) between latitudes y and y_0 that is the result of the integrated surface heat flux between these latitudes. The left-hand side of the last equation is what we refer to as the meridional flux of heat (and, similarly, for the freshwater flux).

The meridional flux may be decomposed into contributions of advection (vT in (17)) and diffusion ($k_h T_y$). Diffusion in this model can be considered a crude representation of the effects of mesoscale eddies, which would tend to break down tight gradients of temperature and salinity. Another possible decomposition of the meridional flux [e.g., *Bryan and Lewis*, 1979, equation (25)] is to divide the advection part into "overturning" and "gyre" contributions. The first is the advection of the zonally averaged temperature by the zonally averaged velocity, corresponding to the contribution of the vertical overturning cell; and the second is the total advection minus the overturning contribution, roughly corresponding to the advection by wind-driven gyres. In our calculations the isopycnal mixing is used rather than the simple horizontal and vertical diffusivities (see appendix), but the preceding discussion still applies with the obvious modifications to the mixing term.

When presenting the meridional flux for separate ocean basins, the starting latitude for the integration, y_0, is taken to be 73.367°N, which roughly corresponds to the latitude of the Bering Strait for the Pacific Ocean and is slightly north of the Denmark Strait for the North Atlantic Ocean. For the global ocean the starting latitude for the integration is the north pole, where the meridional flux vanishes, of course. Note that in the model the freshwater flux at the surface is actually replaced by a virtual salt flux condition, as is commonly done in ocean GCMs [*Huang*, 1993]. As a result, salt flux and freshwater flux are not independent, as they are in the real ocean [*Wijffels et al.*, 1992].

3. RESULTS

3.1. *Standard Model Solution and Implied Fluxes*

Before applying the methodology introduced in the previous section, we use the standard procedure for specifying surface temperature and salinity in order to calculate the implied heat and freshwater fluxes using (1) and (2) with a commonly used value for the restoring coefficients, $\gamma^T = \gamma^S = 1/30\ \mathrm{d}^{-1}$ (run a in Table 1). The results are shown in Figures 2–5. The results shown in Figures 2–4 provide an assessment of the model's performance. The total meridional overturning for the entire world ocean is shown in Figure 2. The results are in general agreement with diagnostic results from much higher resolution models [*Semtner and Chervin*, 1988; *Fujio et al.*, 1992], with the exception of the region immediately adjacent to Antarctica. In the northern hemisphere, over 18 Sv of deep water are formed which flow southward at depths between 2 and 3 km. The upper ocean near the equator is dominated by equatorial upwelling, and a very deep overturning circulation known as the "Deacon cell" exists below the southern hemisphere westerly winds. Figure 2 shows upwelling adjacent to Antarctica, while many other models indicate sinking.

Zonally averaged temperature and salinity are shown in meridional sections in Figure 3. The simulation of the general shape of the thermocline is excellent. In this regard the isopycnal mixing formulation of the model is very important. A test without this feature (results not shown) results in a much thicker and more diffuse thermocline. The salinity fields indicate reasonable agreement in the upper ocean with a good simulation of Antarctic Intermediate Water (AAIW) in the Atlantic.

The corresponding fields of implied air-sea heat flux and net freshwater flux, calculated using (1) and (2), are shown in Figure 4. Both the heat flux and the $E - P$ patterns may be compared to the observational estimates shown in Figures 1*c* and 1*d*. Note that the pattern of Figure 4 for $E - P$

TABLE 1. Summary of All Runs Used in This Study

Run	Data Used	α^T	α^S	γ^T, day^{-1}	γ^S, day^{-1}	$T - T^d$ rms °C	$H - H^d$ rms, W m^{-2}	$S - S^d$ rms, ppt	$(E - P) - (E - P)^d$ rms, cm yr^{-1}	Corresponding Figures
a	T^d, S^d	0	0	1/30	1/30	0.5439	44.12	0.1136	211.20	2, 3
b	all*	0.6	0.9	1/30	1/30	0.8634	31.63	0.3570	69.52	4, 5, 6
c	T^d, S^d	0	0	1/60	1/240	0.8278	34.46	0.3167	112.92	
d	T^d, S^d	0	0	1/30	1/120	0.5064	40.42	0.2181	124.01	
e	T^d, S^d	0	0	1/10	1/30	0.2199	52.68	0.1131	210.30	

Coefficients are defined in the text; α^T and α^S in equations (4) and (5) and γ^T and γ^S in equations (1) and (2). T and S are the model-calculated, upper-level temperature and salinity; H and $[E - P]$ denote the model-calculated heat and freshwater fluxes, respectively. The same quantities with superscript d (e.g., T^d) refer to the corresponding data value.
*H^d, $[E - P]^d$, T^d, and S^d.

includes the implied contribution of river discharge along the continental coastline, since runoff is an important factor in the salinity distribution near shore. The spatial distributions of heat and freshwater fluxes show some significant differences between the climatological flux data (Figures 1*c* and 1*d*) and implied fluxes (Figure 4). It is clear that the patterns of Figure 4 are much more complex than the observational estimates in Figure 1, particularly in regions of western boundary currents and the circumpolar current. This difference in complexity is due to several factors. One is simply that the observational estimates are averaged with respect to space and do not take into account details of the observed sea surface distribution. This is obvious if the *Esbensen and Kushnir* [1981] estimates are compared with the *Isemer and Hasse* [1987] heat flux for the North Atlantic. Another factor is simply a misfit between the model and the imposed surface temperature and salinity data. The temperature and salinity in western boundary current regions, in particular, are strongly affected by the strong transports in these regions. The inability of the coarse ocean model to simulate the large transports needs to be balanced by an unrealistic value of the implied fluxes in order to allow the surface temperature and salinity to still be close to the specified Levitus data. Qualitative agreement between observations and the model seems to be highest in low latitudes away from boundaries.

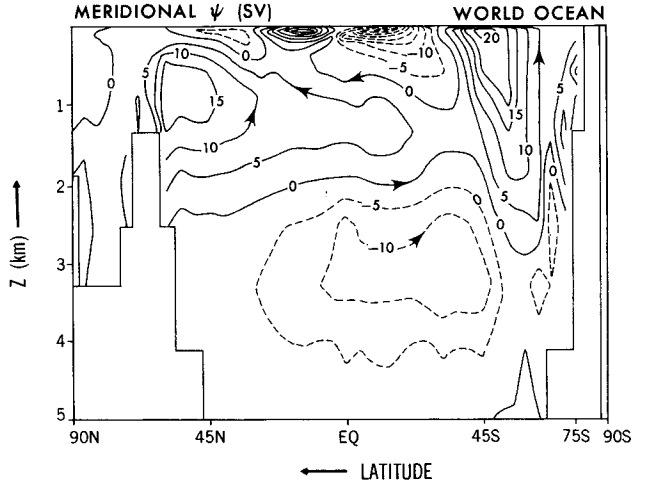

Fig. 2. Results of the "standard" model run (run a in Table 1) obtained by specifying sea surface temperature and sea surface salinity, using restoring times of 30 days and running the model to steady state. Plot shows latitude versus height of the meridional stream function for the global ocean.

For example, the model captures the zone of minimum of $E - P$ just north of the equator in the Pacific and the belt of minimum $E - P$ extending from the Indonesian area diagonally across the South Pacific. It seems that the low-resolution model of this study provides the best fit to surface boundary conditions in open ocean areas, without convective overturning.

While both the implied heat flux and the implied salt flux deviate significantly from the climatological data values, the implied salt flux seems particularly noisy and farther away from the climatological data. The rms difference between the implied and the climatological fluxes (given in Table 1) is 44 W m^{-2} and 211 cm yr^{-1} for the heat and freshwater fluxes, respectively. The rms difference between the heat fluxes is quite large, but within the order of the assumed error level for the climatological heat fluxes (50 W m^{-2}). But the deviation of the rms difference between the freshwater fluxes from the assumed error in the climatological fluxes (50 cm yr^{-1}) is quite large.

The total model meridional transports (Figure 5), including both advection and diffusion, can be compared with those calculated from the climatological flux data and are shown in Figure 1*e*. The poleward heat transport is obtained by integrating the surface heat flux over the ocean with respect to both latitude and longitude (see (17)). As a result, many of the complex details shown in Figure 4 cancel out, and the total transport curves for both heat and moisture are relatively smooth. Comparing the northward heat transport with the estimate shown in Figure 1*e* from the *Esbensen and Kushnir* [1981] data, we find that the most noteworthy discrepancy is the amplitude of northward heat transport in the northern hemisphere. Poleward heat transport in the model is only about one half of that indicated by the data.

Two breakdowns of poleward transport of heat and fresh water are shown in Figure 5. The panels on the left show advection and lateral diffusion separately. Diffusion plays the most significant role in midlatitudes of both hemispheres, but it is particularly important along the circumpolar current front of the southern ocean. Another perspective can be gained by examining the right-hand panels of Figure 5. The advection component of transport is divided into the overturning and gyre components (see discussion following (17)). Note that these two terms often tend to compensate each other. For example, at the equator the wind-driven overturning tends to transport heat away from the equator toward both poles. At the same time the gyres tend to transport back toward the equator. In the southern ocean the "Deacon cell" shown in Figure 2 drives heat toward the equator, but

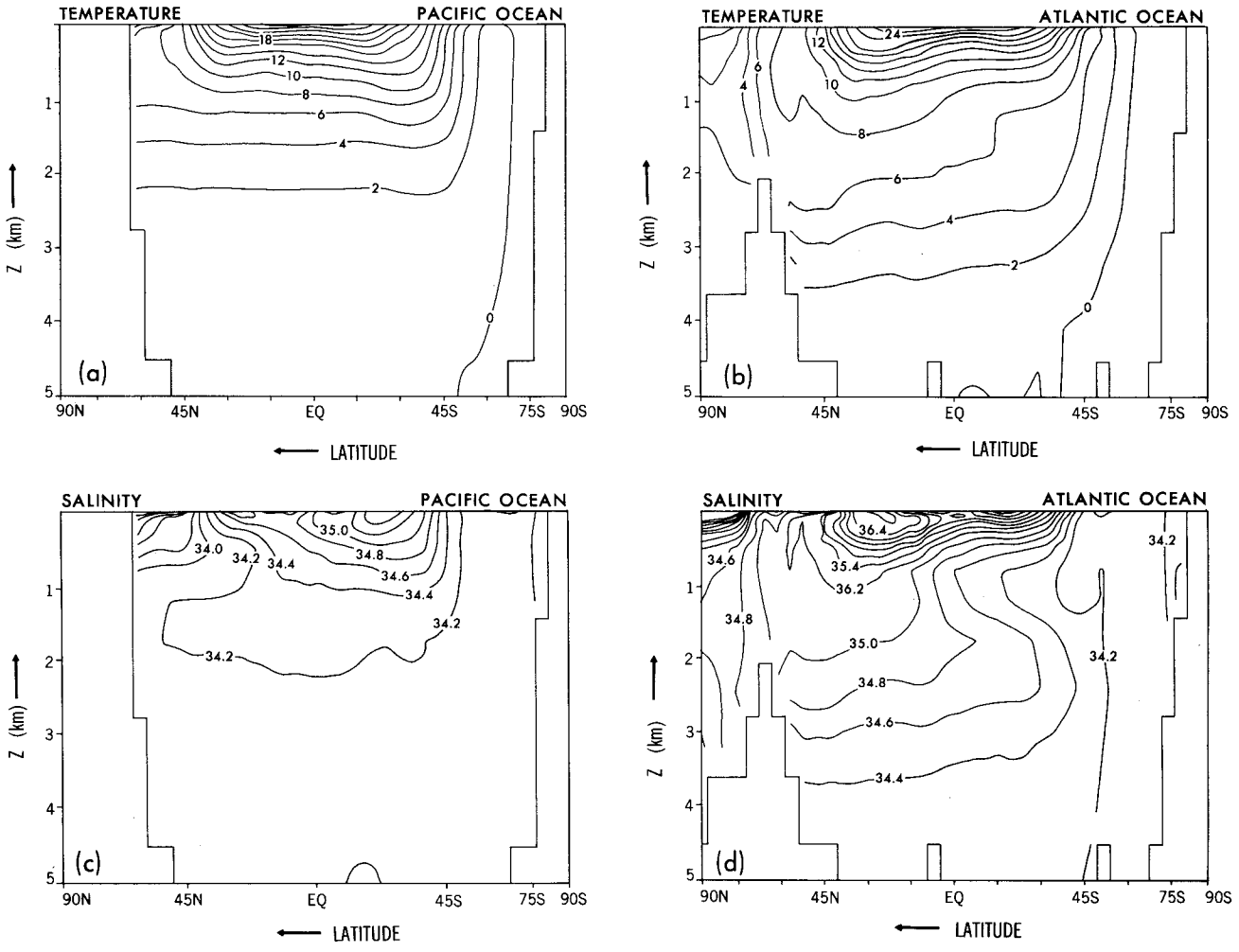

Fig. 3. Same as for Figure 2, with (*a*) Zonally averaged temperature for the Pacific Ocean. (*b*) Zonally averaged temperature for the Atlantic Ocean. (*c*) Zonally averaged salinity for the Pacific Ocean. (*d*) Zonally averaged salinity for the Atlantic Ocean.

it is compensated by departures from the zonal average in velocity and temperature which drive heat toward Antarctica.

The same type of compensation between the overturning and gyre component of the transport does not exist in the northward transport of fresh water. In this case the gyre component appears to be much more important at all latitudes, suggesting that the net poleward transport of fresh water cannot be explained in terms of any simple "conveyor belt" analogy.

Unlike the implied fluxes, the calculated upper level temperature and salinity do not deviate significantly from the data values. The rms difference between the calculated temperature and the Levitus data is only about 0.5°C, about one half of the assumed error level in the temperature data. The rms deviation of the salinity from the data is only 0.1 ppt, significantly smaller than the assumed error of 0.25 ppt.

3.2. *"Optimal" Solution for the Air-Sea Fluxes*

The results presented above raise the question of whether it might be possible to allow larger deviations from the surface temperature and salinity data, and therefore improve the fit to the climatological flux data. We try next to answer this question by using the methodology presented in section 2.1 to calculate the air-sea fluxes based on both the surface properties and the climatological flux data (run b in Table 1). We first wish to emphasize that the interior solution for the temperature, salinity, and velocity field is hardly different from those of the standard solution shown in Figures 2–4. The results for the air-sea fluxes are shown in Figure 6. The general appearance of the fluxes is much smoother than that of the implied fluxes in Figure 4, and the rms difference between the calculated flux and the data value is smaller than that for the implied fluxes (especially for the freshwater flux; see Table 1). The better fit to the climatological flux data is balanced by an increase in the rms difference between the surface temperature and salinity data and these values calculated by the model. Thus the model deviated further from the temperature and salinity data in order to decrease the distance from the climatological flux data. The final solution is such that the deviations from all data values are of the order of magnitude of the specified errors for the various data fields. The structure of the rms residuals indicates that the method was able to use each data type in accordance with its expected accuracy and to stay as much as possible within the specified error bars.

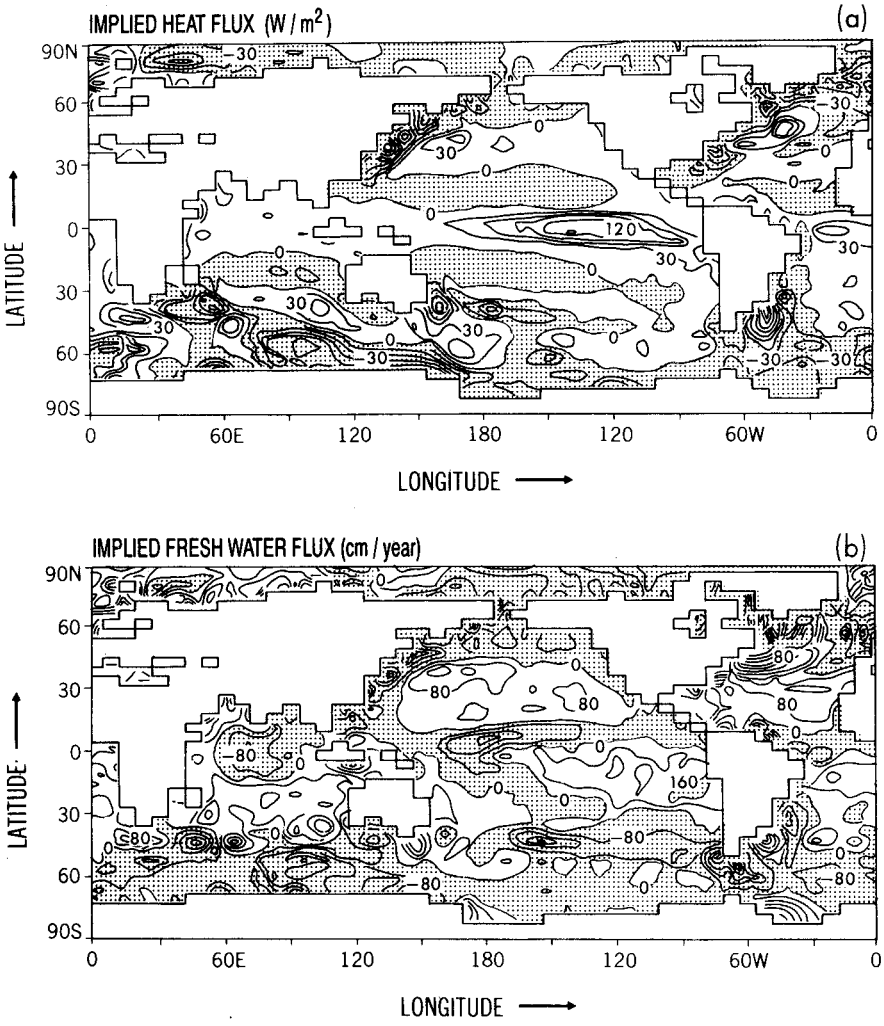

Fig. 4. Implied air-sea heat and freshwater fluxes from the standard model solution.

The general ability of the solution to balance rms distances to the various data types confirms our expectation that the approach used here is closely related to the optimization approach used as the motivation for deriving (4) and (5) for the fluxes.

Consider next the meridional fluxes of heat and fresh water calculated for the "optimal" solution of run b in Table 1. There seem to be many differences between the patterns of surface heat flux obtained in this run and those in the run in which both the surface temperature and salinity are specified. These differences are very obvious when Figure 4 is compared with Figure 6. With this result in mind one would expect a priori that there would also be significant differences in the poleward transport of heat in the two solutions. Poleward heat transport for the optimal run is shown in Figure 7 and can be compared with the heat transport values for run a given in Figure 5. Surprisingly, it is difficult to distinguish any significant differences between the poleward transport of heat and water in the two cases. A closer examination of the implied (Figure 4) versus optimal (Figure 6) fluxes shows that the differences between the two fields are mostly in the very small scale (1 to 2 grid points) patterns that are present only in the implied fluxes. Evidently, these small-scale patterns do not contribute significantly to the area integral used to obtain the meridional fluxes (right-hand side of (17)) because of their small area. To some extent the differences in local heat and water flux in the implied and optimal solutions also tend to cancel out when integrated with respect to latitude and longitude as is required to obtain the poleward transports.

In Table 2 the results of the optimal run shown in Figure 7 are compared with earlier model results [*Bryan*, 1982] and estimates from observations. The *Bryan* [1982] results are actually based on a world ocean modeling study described more fully by *Bryan and Lewis* [1979]. The *Bryan and Lewis* [1979] model was similar in many respects to the present model, except that it included seasonal variations. It was forced by the *Levitus* [1982] temperature and salinity data at the upper boundary, and the wind stress data are the same as those used in the present study. Comparing the results shown in Table 2, we see that transports predicted in the optimal run without seasonal variations are very much like those of earlier model studies. In the North Atlantic, model heat transport is only 50% of that indicated by *Esbensen and Kushnir* [1981] and of direct measurements by *Bryden and Hall* [1980]. In the North Atlantic there is a better agreement between *Baumgartner and Reichel*'s [1975] results and model results for water transport, but there is a significant

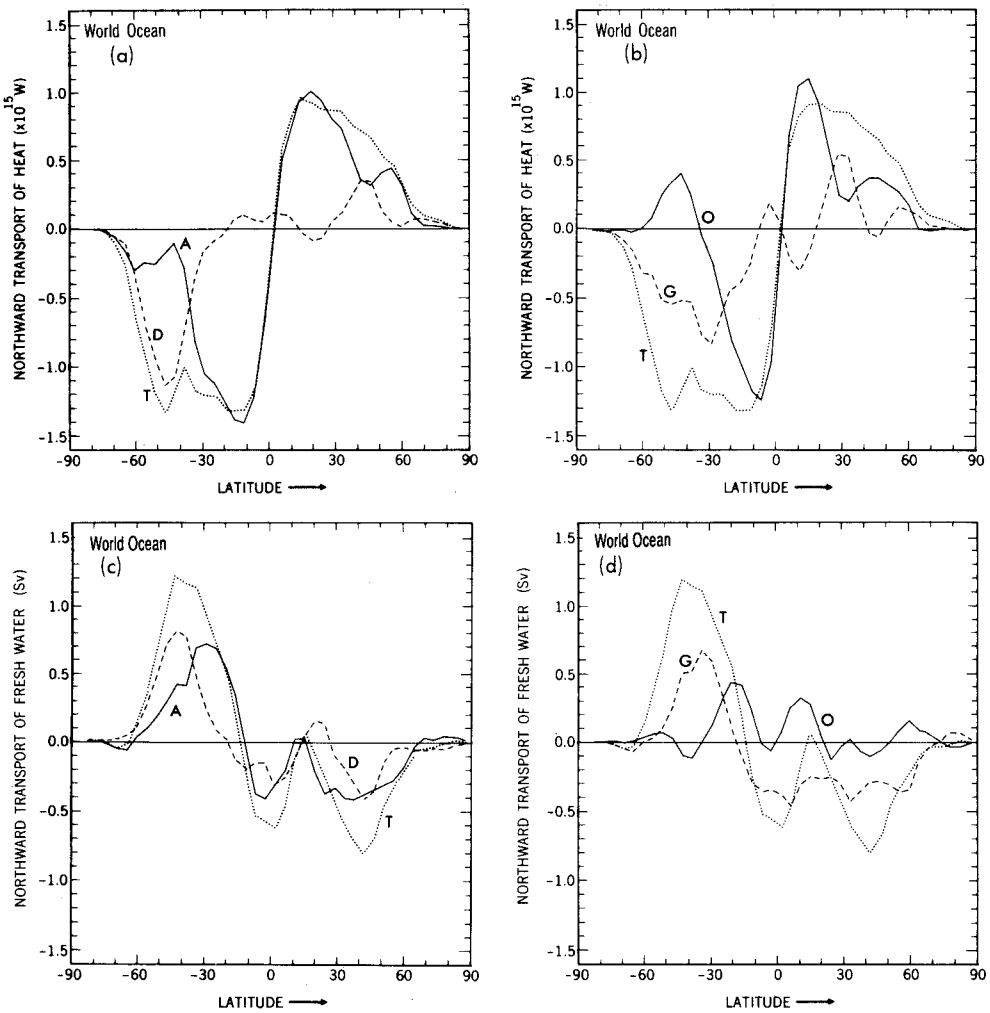

Fig. 5. Meridional heat (Figures 5*a* and 5*b*) and freshwater (Figures 5*c* and 5*d*) fluxes for the global ocean obtained from the standard case (run a in Table 1). Figures 5*a* and 5*c* show the advection (solid line marked A), diffusion (dashed line D) and total (dotted line T) contribution to the meridional flux. Figures 5*b* and 5*d* show the decomposition of the advection into the gyre (dashed line G) and overturning (solid line O) contribution, as well as the total flux (dotted line T).

discrepancy in the South Atlantic. Baumgartner and Reichel indicate a net loss of water to the atmosphere in the Atlantic between 40°N and 30°S, which is 2 or 3 times as great as that indicated by the models.

In the North Pacific the discrepancy in poleward heat transport between the models and estimates from data is similar to that in the North Atlantic. On the other hand, the agreement of models and data on heat transport for the combined effect of the Pacific and Indian oceans in the southern hemisphere is remarkably good. Net water transport of the Pacific and Indian oceans also agrees quite well with the *Baumgartner and Reichel* [1975] estimates in the northern hemisphere.

For the entire world ocean we see that poleward heat transport is about 50% of that estimated by surface heat balance in the northern hemisphere, but it is just about the same in the southern hemisphere. Differences between the model and observations in poleward water transport for the South Atlantic and the combined South Pacific and Indian oceans tend to cancel each other. As a result, there is reasonable agreement between the optimal run and water balance zonal net estimates in both the northern and southern hemispheres.

The relative importance of the mean meridional overturning and horizontal gyres in poleward transport can be seen in Figures 7*b* and 7*d*. In the Pacific and Indian ocean sector, overturning is important in the vicinity of the equator, with the gyre component becoming more important in midlatitudes. This is true for the transport of both heat and fresh water. In the Atlantic Ocean, overturning associated with the thermohaline circulation plays the dominant role as might be expected. The "gyre" component of the meridional circulation estimated with our model may be expected to experience significant uncertainties due to the inability of the model to resolve the large transports of the western boundary currents.

We are now in a position to return to the important issue of model validation using our approach. We have seen that while a better fit to the spatial structure is possible to obtain by increasing the distance to the observed SST and SSS, it is not possible to significantly improve the meridional fluxes calculated by the model this way. The inability of the model

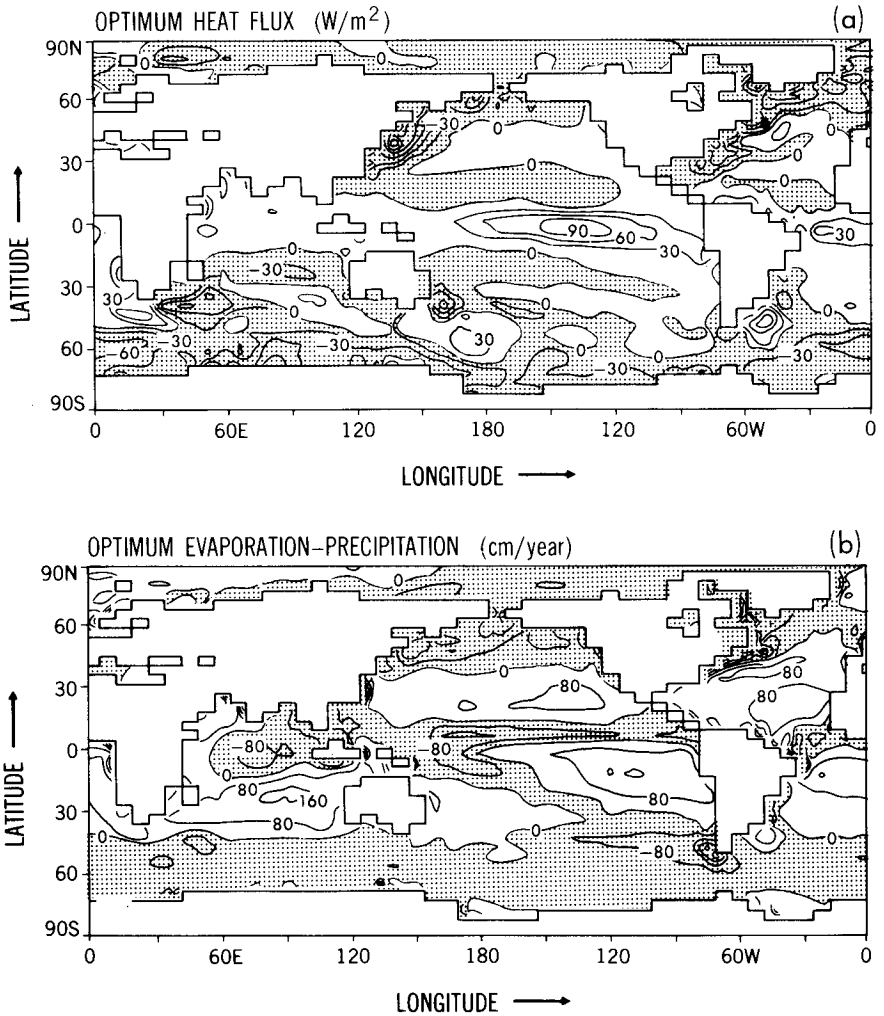

Fig. 6. "Best estimates" for the heat and freshwater fluxes (run b in Table 1) obtained by combining SST and SSS data with the climatological heat and freshwater flux estimates.

to correctly simulate the meridional fluxes seems to be due to the internal model dynamics. Examining the meridional circulation in the model (Figure 2), we note that much of the deep water formed in the northern hemisphere upwells north of 30°N, leaving a meridional cell of less than 10 Sv south of 25°N. Such meridional circulation contradicts the observational evidence of *Hall and Bryden* [1982], for example, who find a 17-Sv meridional cell in the North Atlantic alone at 24°N. The weaker meridional cell calculated by the model seems to be the main reason for the discrepancy between the model meridional fluxes of heat and those deduced from the climatological fluxes. It is worthwhile mentioning that other reasons for the difficulty with the meridional fluxes are possible, such as the inability of this coarse model to resolve the large transports of the western boundary current and corresponding sharp temperature gradients.

The residual fields (the differences between the data values and the fields calculated by the model) are shown in Figure 8. In most regions of the world ocean the deviation of all fields (temperature, salinity, heat fluxes, and freshwater fluxes) from the data is reasonable and roughly of the order of magnitude of the expected errors. However, deviations from the data values are significantly larger than the error estimates in some restricted regions, notably western boundary regions. In these regions the temperature and the calculated heat flux strongly deviate from the *Levitus* [1982] and *Esbensen and Kushnir* [1981] data sets, respectively. Similar misfits are observed for the salinity and freshwater fluxes. These larger deviations from the data values in western boundary regions can probably be explained by the limitations of the coarse model there, as discussed in the section 3.1.

We have seen several times that the value of 1/30 d^{-1} for the restoring coefficients used to calculate the implied fluxes may be too large, especially for the salinity. Too-large values for the restoring coefficients should not have a significant effect on our optimal estimates for the fluxes. Such a large salinity-restoring coefficient results in a large error estimate in (9) for $(E - P)^{SSS}$, which in turn results in α^S being close to 1 (see (7)). When the value of α^S is close to 1, the noisy and unrealistic implied freshwater flux calculated as a result of the large restoring coefficient, is downweighted compared with the climatological fresh water flux data, leaving our optimal estimate unaffected by the bad estimate for the

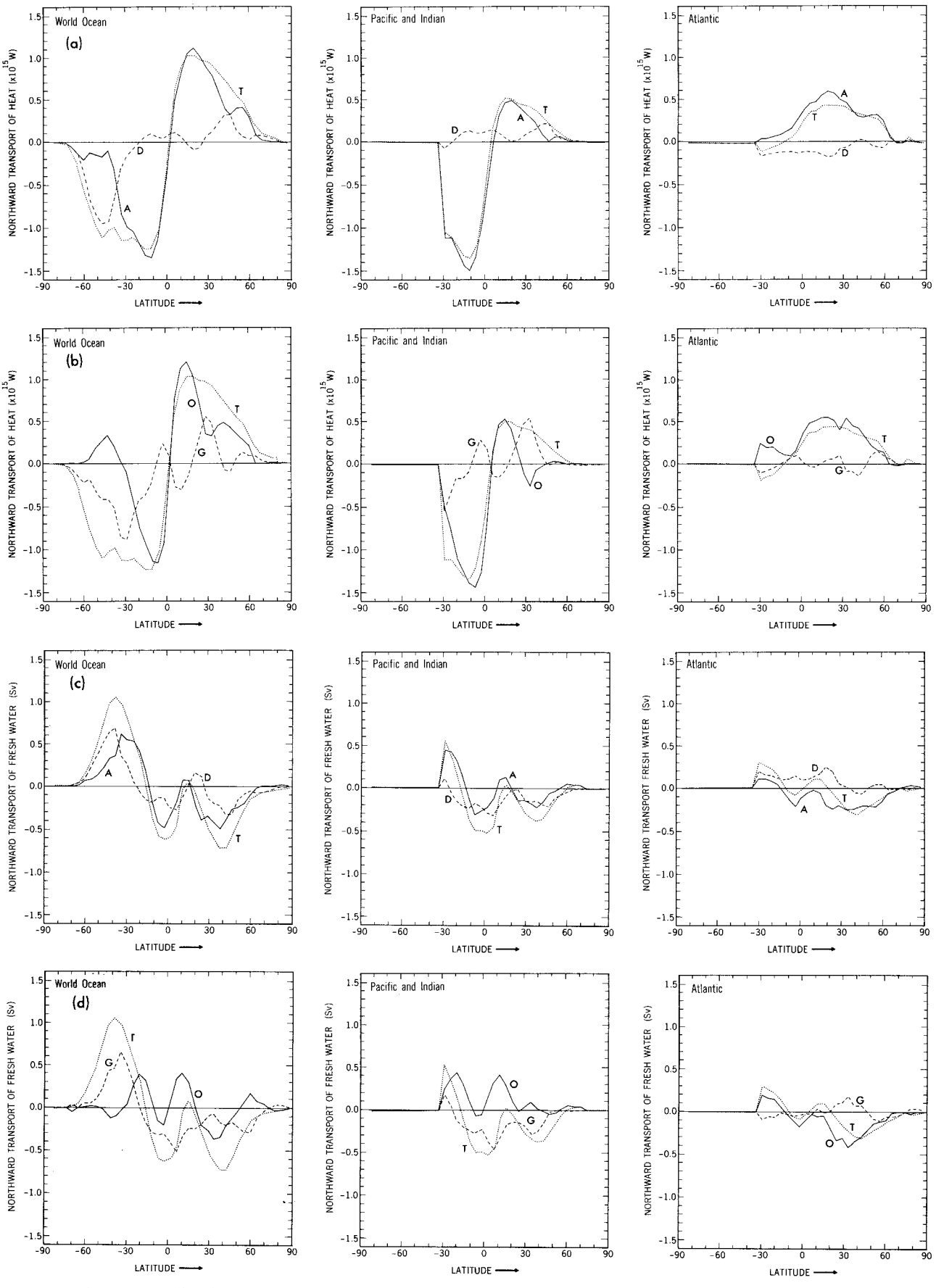

Fig. 7. Meridional heat and freshwater fluxes obtained from the best estimates (run b in Table 1). Each meridional flux is shown for the global ocean (left column), for the Indian and Pacific oceans (combined, middle column), and for the Atlantic Ocean (right column). Figures 7*a* and 7*c* show that heat and freshwater fluxes are decomposed into contributions due to advection (solid lines marked A) and diffusion (dashed lines marked D), with the total flux also shown (dotted lines marked T). Figures 7*b* and 7*d* show the decomposition of the advection part of the flux into the gyre (dashed line marked G) and overturning (solid line marked O) contribution, as well as the total flux (dotted line marked T).

implied flux. It is interesting, however, to examine if a better fit between the climatological fluxes and the implied fluxes may be obtained by simply reducing the value of the restoring coefficients. For this purpose, we have carried out a number of additional experiments, in which surface properties are specified using different choices for the restoring coefficients γ^T and γ^S and without using the climatological flux estimates. The results are given in Table 1, runs c, d, and e. Run c amounts to doubling the restoring time for the temperature to 60 days and increasing that of the salinity by a factor of 4. The results indicate an improvement in the fit to the climatological flux relative to run a, in which a 30-day value was used for both T and S. The rms distance to the climatological fluxes was reduced from 44 to 34 W m^{-2} for the heat flux and from 211 to 112 cm yr^{-1} for the freshwater flux. Note, however, that using the methodology described in section 3.1 (run b), the rms difference for the freshwater fluxes was reduced to 69 cm yr^{-1} by deviating from the surface salinity by about as much as in run c. Clearly, a reduction of the restoring coefficients from 1/30 days^{-1} improves the fit to the climatological fluxes by allowing larger deviations from the surface properties. However, an even better fit to the flux data is obtained by using (1) and (2) at the cost of about the same deviation from the surface temperature and salinity data. Runs d and e merely strengthen the conclusion that by modifying the restoring coefficients used to calculate the implied fluxes, one can improve or worsen the fit to the climatological fluxes.

It would obviously be most useful to have a physically motivated algorithm for calculating the restoring coefficients that are presently chosen empirically and, perhaps, somewhat arbitrarily. Perhaps the simple error analysis presented in (8) and (9) can serve as a first step in this direction. The dynamical consequences of using too-large values for the restoring coefficients are discussed by *Tziperman et al.* [1993], who emphasize, in particular, the effect of these coefficients on the stability of the thermohaline circulation. They also propose a simple criterion for choosing these

TABLE 2. Heat and Water Transports in This Study Compared With Previous Estimates

	Northward Heat Transport, 10^{15} W		Northward Water Transport, 10^6 m^3 s^{-1}	
	25°N	25°S	40°N	50°S
Atlantic Ocean				
Optimal run	0.4	−0.1	−0.3	0.2
Bryan [1992]	0.5	0.2	−0.2	0.1
Esbensen and Kushnir [1981]	0.9	−0.1	...	...
Baumgartner and Reichel [1975]	...	...	−0.3	0.5
Bryden and Hall [1980]	1.1 ± 0.3	...	...	...
Pacific and Indian Oceans				
Optimal run	0.4	−1.1	−0.4	0.5
Bryan [1982]	0.4	−1.0	−0.3	0.3
Esbensen and Kurhnir [1981]	0.9	−1.1	...	...
Baumgartner and Reichel [1975]	...	...	−0.4	0.1
Bryden et al. [1991]	1.8 ± 0.3	...	...	...
World Ocean				
Optimal run	0.8	−1.2	−0.7	0.7
Bryan [1982]	0.9	−0.8	−0.5	0.4
Esbensen and Kushnir [1981]	1.8	−1.2	...	...
Baumgartner and Reichel [1975]	...	...	−0.7	0.6
Peixoto and Oort [1983]	...	...	−0.7	0.7

See text for details.

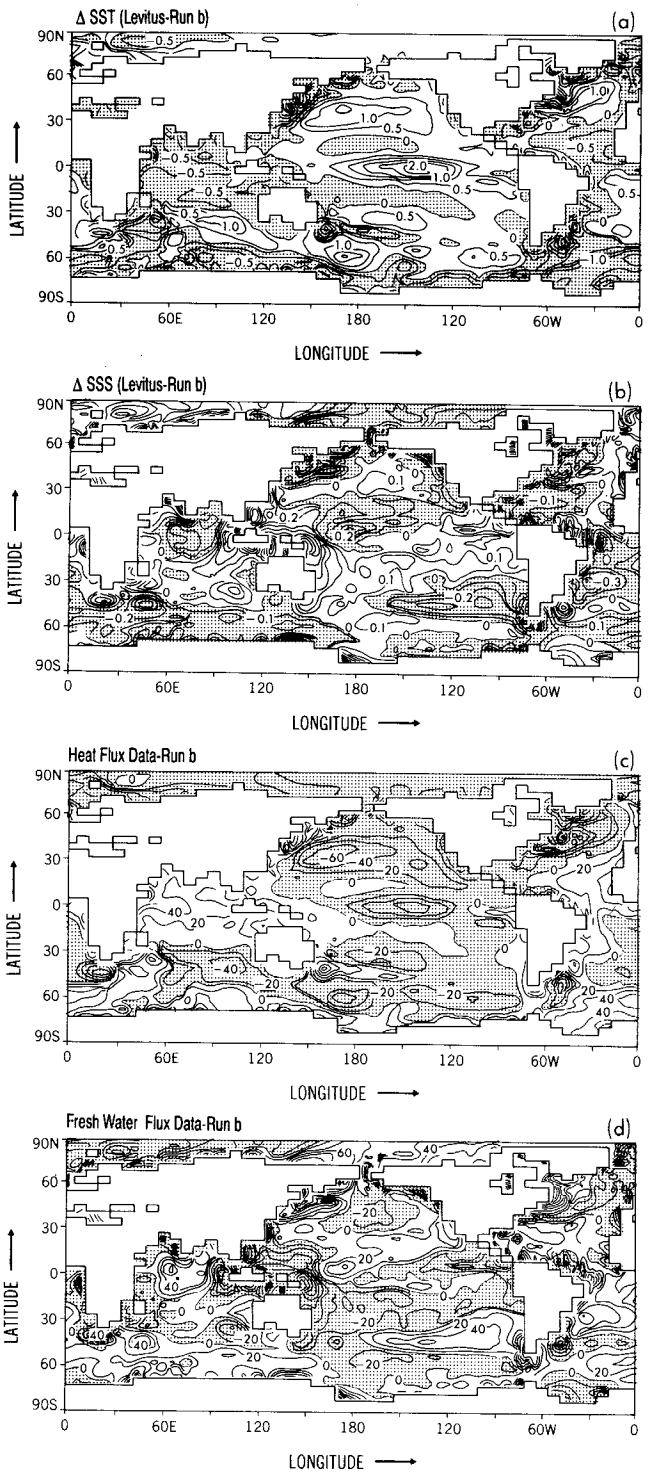

Fig. 8. Residual fields from run b in Table 1. (*a*) Levitus data temperature at the upper level minus the model solution at this depth. (*b*) Same as Figure 8*a*, for salinity. (*c*) The climatological heat flux data of *Esbensen and Kushnir* [1981] minus the best estimate for the air-sea heat flux calculated in run b. (*d*) The climatological freshwater flux data of Esbensen and Kushnir minus the best estimate for the freshwater flux.

coefficients when specifying the SST and SSS without using climatological flux data.

4. CONCLUSIONS

We presented and demonstrated a simple method for estimating air-sea fluxes of heat and fresh water, with the aid of a general circulation model, using both sea surface temperature and salinity data and climatological air-sea flux data.

The method was motivated by a least squares optimization problem in which the various data sets are combined to form an optimal solution for the air-sea fluxes. While the method shown here does not provide optimal estimates in the least squares sense, its results may be reasonably close to such an optimal estimate. An air-sea flux estimate obtained by this simple method may be used to initialize a least squares optimization based on a nonlinear inverse method such as the adjoint method. Such an initialization is important because the gradient-based optimization methods may fail if started too far from the optimal solution, because of the possible existence of multiple local minima of the cost function that is minimized in the optimization [*Tziperman et al.*, 1992].

The proposed method was applied to a coarse resolution global primitive equations model, in order to estimate the global air-sea fluxes of heat and fresh water. The resulting air-sea fluxes seem smoother and closer to the climatological flux estimates than the implied air-sea fluxes obtained from the GCM by simply specifying the surface temperature and salinity. In most regions of the world ocean the deviation of the calculated surface properties and the air-sea fluxes from the corresponding climatological data sets was within the assumed a priori errors of the climatological data. These deviations were quite large, however, in regions of strong western boundary currents, indicating that the various data fields and the model dynamics are not consistent with each other in these regions. The inconsistencies between the model and data in western boundary current regions are most probably related to the inability of the coarse resolution GCM to appropriately represent the large transports and strong horizontal advection of the western boundary currents.

The meridional fluxes of heat and fresh water calculated using the proposed methodology (our "optimal" solution) were presented for the global ocean as well as for the different ocean basins. In contrast with the spatial distribution of the fluxes that seem significantly different from the implied fluxes, the optimal meridional fluxes were quite similar to those derived from the implied fluxes. By allowing the model to further deviate from the specified surface temperature and salinity, our method tends to simply smooth the air-sea fluxes calculated by the GCM, but leave the large-scale spatial distribution roughly unchanged. We concluded that the inability of the present approach to improve the meridional fluxes of heat and fresh water is probably due to the limitations of the model itself. In particular, the meridional circulation in the model seems to be too weak at midlatitudes, which may be the reason for the inconsistencies between the model meridional fluxes and those deduced from climatological flux estimates. The strong constraint imposed on the meridional heat flux by the model meridional circulation has important implications for the calculation of air-sea fluxes by inverse methods. We feel that in order for an inverse model based on a GCM to be able to calculate the air-sea fluxes correctly, the meridional circulation in the GCM must be correct. This can be expected to be a major difficulty in the near future, as coarse resolution GCMs such as the one used here often produce a too-weak meridional circulation at midlatitudes.

Overall, the results of the present study seem encouraging and suggest that it might be useful to apply the present method to higher-resolution models. The use of higher resolution may be expected to result in a better fit of model results and data in western boundary regions and in improved fit to meridional fluxes obtained from other sources.

APPENDIX: CLOSURE APPROXIMATIONS OF THE MODEL

The representation of subscale mixing is somewhat different from that in previous studies with the Geophysical Fluid Dynamics Laboratory model [e.g., *Bryan and Lewis*, 1979]. Lateral diffusion in a model with horizontal coordinates can result in spurious mixing across horizontal surfaces in strongly baroclinic regions such as the Gulf Stream. In reality, time-dependent motions associated with baroclinic instability do cause mixing across time-averaged isopycnal surfaces, but it is important not to exaggerate this effect in ocean circulation models of low horizontal resolution. An isopycnal coordinate system avoids this difficulty, but at the added cost of the complexity associated with a semi-Lagrangian coordinate system. An improvement can be made in the context of a z coordinate model by rotating the mixing tensor so that the largest component is in a plane parallel to isopycnal surfaces, as suggested by *Redi* [1982]. In the present model, isopycnal mixing is combined with the conventional mixing of a z coordinate model, which we call "background" mixing. In effect, mixing is partially rotated to align with density surfaces. The motivation is to simulate the effects of baroclinic eddies, which mix properties in a plane that is inclined with respect to the horizontal, but that has less of a slope than the time-averaged density surfaces.

The conservation equations for temperature and salinity are

$$d/(dt)(T,\ S) = (Q,\ \sigma),$$

where Q and σ represent the effects of mixing by unresolved scales of motion. Using a tensor notation, the mixing terms for temperature and salinity may be written

$$(Q,\ \sigma) = \sum_{ij} \partial_i[K_{ij}\partial_j(T,\ S)], \qquad \text{(A1)}$$

where i and j are summed over the 3 spatial coordinates. For simplicity we will write the mixing tensor in terms of a local Cartesian coordinate rather than the full spherical coordinates of the model. The full mixing tensor is given by *Redi* [1982] with the addition of "background" mixing.

TABLE A1. Parameters of the Model

Parameter	Symbol	Value
Horizontal viscosity	A_{MH}	2.5×10^5 m^2 s^{-1}
Vertical viscosity	A_{MV}	5.0×10^{-3} m^2 s^{-1}
Lateral diffusion	A_L $(z = 0)$	5.0×10^3 m^2 s^{-1}
Horizontal diffusion ratio	ε_2	0.3
Vertical diffusion ratio	ε_3 $(z = 0)$	0.6×10^{-8}
Maximum slope	SL	1/150

Diffusion ratios are with respect to A_L at $z = 0$.

Acknowledgments. This work was done during a visit of E.T. to the Geophysical Fluid Dynamics Laboratory. E.T. is partially supported by the Faivovich Foundation at the Weizmann Institute and by grant 89-00408 from the United States–Israel Binational Science Foundation. We are grateful to Keith Dixon, Bonnie Samuels, and Robert Toggweiler for many useful discussions. Department of Environmental Sciences and Energy Research, Weizmann Institute of Science, contribution 45.

$$\mathsf{K} = \frac{A_L}{1+\delta^2}\begin{bmatrix} \varepsilon_2 + 1 + (\rho_y^2 + \varepsilon_3\rho_x^2)/\rho_z^2 & (\varepsilon_3 - 1)\rho_x\rho_y\rho_z^{-2} & (\varepsilon_3 - 1)\rho_x\rho_z^{-1} \\ \cdots & \varepsilon_2 + 1 + (\rho_x^2 + \varepsilon_3\rho_y^2)\rho_z^{-2} & (\varepsilon_3 - 1)\rho_y\rho_z^{-1} \\ \cdots & \cdots & \varepsilon_3 + \delta^2 \end{bmatrix}. \quad \text{(A2)}$$

The right-hand side of (A2) is a symmetric matrix. The subscripts x, y, and z indicate partial differentiation; A_L is the coefficient of lateral diffusion; ε_2 is the ratio of background horizontal to lateral isopycnal diffusion; ε_3 is the ratio of background vertical diffusion to lateral isopycnal diffusion; and δ is the slope of isopycnals.

For practical purposes, (A2) can be simplified considerably. The ratio ε_3 is much less than unity. The slope of isopycnal surfaces that can be resolved by the model is also much less than one. Neglecting small terms,

$$\mathsf{K} = A_L\begin{bmatrix} 1 + \varepsilon_2 & 0 & -\rho_x\rho_z^{-1} \\ \cdots & 1 + \varepsilon_2 & -\rho_y\rho_z^{-1} \\ \cdots & \cdots & \varepsilon_3 + \delta^2 \end{bmatrix}.$$

Note that if only those terms involving background mixing are retained, we recover the usual mixing tensor for ocean models with horizontal coordinates.

The mixing tensor formulation places a limitation on the time step of the model in the case of very steep slopes, which cause the lateral mixing tensor to be rotated into a nearly vertical plane. In that case the large implied mixing across the relatively closely spaced vertical levels of the model places a severe limitation on the time step. This is avoided by placing a limit on the slope to which the tensor can be rotated, SL, which is specified with other diffusion and viscosity parameters in Tables A1 and A2.

TABLE A2. Lateral Diffusion and Vertical Diffusion Ratio as a Function of Depth

Depth, m	$A_L(z)/A_L(0)$	$\varepsilon_3(z)/\varepsilon_3(0)$
25	1	1.0
85	0.89	1.0
169	0.80	1.0
295	0.66	1.0
483	0.55	1.0
755	0.44	1.1
1131	0.37	1.1
1622	0.32	1.3
2228	0.29	2.9
2935	0.26	4.0
3721	0.23	4.2
4566	0.20	4.3

REFERENCES

Baumgartner, A., and E. Reichel, *The World Water Balance*, 179 pp., Elsevier, New York, 1975.

Bryan, K., Measurement of meridional heat transport by ocean currents, *J. Geophys. Res.*, *67*, 3403–3414, 1962.

Bryan, K., A numerical method for the study of the circulation of the world ocean, *J. Comput. Phys.*, *4*, 347–376, 1969.

Bryan, K., Poleward heat transport by the oceans: Observations and models, *Annu. Rev. Earth Planet. Sci.*, *10*, 15–38, 1982.

Bryan, K., Accelerating the convergence to equilibrium of ocean-climate models, *J. Phys. Oceanogr.*, *14*, 666–673, 1984.

Bryan, K., and L. J. Lewis, A water mass model of the world ocean, *J. Geophys. Res.*, *84*, 2503–2517, 1979.

Bryden, H., and M. Hall, Heat transport by ocean currents across 25 N latitude in the Atlantic, *Science*, *207*, 884–886, 1980.

Bryden, H., D. H. Roemmich, and J. A. Church, Ocean heat transport across 24 N in the Pacific, *Deep Sea Res.*, *38*, 297–324, 1991.

Coachman, L. K., and K. Aagaard, Transports through Bering Strait: Annual and interannual variability, *J. Geophys. Res.*, *93*, 15,535–15,539, 1988.

Cox, M. D., A primitive equation 3 dimensional model of the ocean, *Tech. Rep. 1*, Ocean Group, Geophys. Fluid Dyn. Lab., Princeton Univ., Princeton, N. J., 1984.

Esbensen, S. K., and Y. Kushnir, The heat budget of the global ocean: An atlas based on estimates from surface marine observations, *Rep. 29*, Climate Res. Inst., Oreg. State Univ., Corvallis, 1981.

Ezer, T., and G. L. Mellor, A numerical study of the variability and separation of the Gulf Stream, induced by surface atmospheric forcing and lateral boundary flows, *J. Phys. Oceanogr.*, *22*, 660–682, 1992.

Fujio, S., T. Kadowaki, and N. Imasato, World ocean circulation diagnostically derived from hydrographic and wind stress fields, 1, The velocity field, *J. Geophys. Res.*, *97*, 11,163–11,176, 1992.

Ghil, M., and P. Malanotte-Rizzoli, Data assimilation in meteorology and oceanography, in *Advances in Geophysics*, vol. 33, edited by B. Saltzman, pp. 141–266, Academic, San Diego, Calif., 1991.

Hall, M. M., and H. L. Bryden, Direct estimates and mechanisms of ocean heat transport, *Deep Sea Res.*, *29*, 339–359, 1982.

Hellerman, S., and M. Rosenstein, Normal monthly wind stress over the world ocean with error estimates, *J. Phys. Oceanogr.*, *13*, 1093–1104, 1983.

Huang, X. R., Real fresh water flux as a natural boundary condition for the salinity balance and thermohaline circulation forced by evaporation and precipitation, *J. Phys. Oceanogr.*, in press, 1993.

Isemer, H. J., and L. Hasse, *The Bunker Climate Atlas of the North Atlantic Ocean*, vol. 2, *Air-Sea Interactions*, 252 pp., Springer-Verlag, New York, 1987.

Levitus, S., Climatological atlas of the world ocean, *Prof. Pap. 13*, 173 pp., Natl. Oceanic and Atmos. Admin., Boulder, Colo., 1982.

Manabe, S., R. J. Stouffer, M. J. Spelman, and K. Bryan, Transient

response of a coupled ocean-atmosphere model to gradual changes of atmospheric CO_2, I, Annual mean response, *J. Clim.*, *4*, 785–818, 1991.

Mercier, H., A study of the time averaged circulation in the western North Atlantic by simultaneous nonlinear inversion of hydrographic and current meter data, *Deep Sea Res.*, *36*, 297–313, 1989.

Oberhuber, J. M., An atlas based on the COADS data set: The budgets of heat, buoyancy and turbulent kinetic energy at the surface of the global ocean, *Rep. 15*, Max-Planck-Inst. für Meteorol., Hamburg, Germany, 1988.

Peixoto, J. P., and A. H. Oort, The atmospheric branch of the hydrological cycle and climate, in *Variations in the Global Water Budget*, edited by A. Street-Perrot, M. Beran, and R. Ratcliffe, 518 pp., D. Reidel, Norwell, Mass., 1983.

Redi, M. H., Oceanic isopycnal mixing by coordinate rotation, *J. Phys. Oceanogr.*, *12*, 1154–1158, 1982.

Sarmiento, J. L., and K. Bryan, An ocean transport model for the North Atlantic, *J. Geophys. Res.*, *87*, 394–408, 1982.

Semtner, A. J., An oceanic general circulation model with bottom topography, *Tech. Rep. 9*, 99 pp., Dep. of Meteorol., Univ. of Calif., Los Angeles, 1974.

Semtner, A. J., Jr., and R. M. Chervin, A simulation of the global ocean circulation with resolved eddies, *J. Geophys. Res.*, *93*, 15,502–15,522, 1988.

Stouffer, R. J., S. Manabe, and K. Bryan, Interhemispheric asymmetry in climate response to a gradual increase of atmospheric CO_2, *Nature*, *342*, 660–662, 1989.

Tally, L. D., Meridional heat transport in the Pacific Ocean, *J. Phys. Oceanogr.*, *14*, 231–241, 1984.

Tziperman, E., W. C. Thacker, R. B. Long, S.-M. Hwang, and S. Rintoul, Oceanic data analysis using a general circulation model, II, A North Atlantic model, *J. Phys. Oceanogr.*, *22*, 1458–1485, 1992.

Tziperman, E., J. R. Toggweiler, Y. Feliks, and K. Bryan, Instability of the thermohaline circulation with respect to mixed boundary conditions: Is it really a problem for realistic models?, *J. Phys. Oceanogr.*, in press, 1993.

Wijffels, E. S., R. W. Schmitt, H. Bryden, and A. Stigebrandt, Transport of fresh water by the oceans, *J. Phys. Oceanogr.*, *22*, 155–162, 1992.

Wunsch, C., An eclectic Atlantic Ocean circulation model, 1, The meridional flux of heat, *J. Phys. Oceanogr.*, *14*, 1712–1733, 1984.

K. Bryan, Geophysical Fluid Dynamics Laboratory, Princeton University, Princeton, NJ 08542.

E. Tziperman, Environmental Sciences, Weizmann Institute of Science, Rehovot, 76100, Israel.

(Received October 30, 1992;
revised February 11, 1993;
accepted March 24, 1993.)